NeuroImage 266 (2023) 119805

Contents lists available at ScienceDirect

NeuroImage

journal homepage: www.elsevier.com/locate/neuroimage

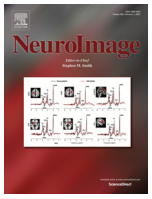

Corticospinal excitability is highest at the early rising phase of sensorimotor μ-rhythm

Christoph Zrenner[a,b,c,d,*], Gábor Kozák[d,e], Natalie Schaworonkow[f], Johanna Metsomaa[d,g], David Baur[d,e], David Vetter[d,e], Daniel M. Blumberger[a,b], Ulf Ziemann[d,e,*], Paolo Belardinelli[d,h]

[a] Temerty Centre for Therapeutic Brain Intervention, Centre for Addiction and Mental Health, Toronto, ON, Canada
[b] Department of Psychiatry, University of Toronto, Toronto, ON, Canada
[c] Institute for Biomedical Engineering, University of Toronto, Toronto, ON, Canada
[d] Department of Neurology & Stroke, University of Tübingen, Germany
[e] Hertie Institute for Clinical Brain Research, University of Tübingen, Germany
[f] Ernst Strüngmann Institute for Neuroscience in Cooperation with Max Planck Society, Frankfurt am Main, Germany
[g] Department of Neuroscience and Biomedical Engineering, Aalto University School of Science, Espoo, Finland
[h] CIMeC, Center for Mind/Brain Sciences, University of Trento, Trento, Italy

ARTICLE INFO

Keywords:
EEG
TMS
MEP
Corticospinal
Excitability
Oscillations
Phase
Sensorimotor
μ-rhythm
Alpha

ABSTRACT

Alpha oscillations are thought to reflect alternating cortical states of excitation and inhibition. Studies of perceptual thresholds and evoked potentials have shown the scalp EEG negative phase of the oscillation to correspond to a short-lasting low-threshold and high-excitability state of underlying visual, somatosensory, and primary motor cortex. The negative peak of the oscillation is assumed to correspond to the state of highest excitability based on biophysical considerations and considerable effort has been made to improve the extraction of a predictive signal by individually optimizing EEG montages. Here, we investigate whether it is the negative peak of sensorimotor μ-rhythm that corresponds to the highest corticospinal excitability, and whether this is consistent between individuals.

In 52 adult participants, a standard 5-channel surface Laplacian EEG montage was used to extract sensorimotor μ-rhythm during transcranial magnetic stimulation (TMS) of primary motor cortex. Post-hoc trials were sorted from 800 TMS-evoked motor potentials (MEPs) according to the pre-stimulus EEG (estimated instantaneous phase) and MEP amplitude (as an index of corticospinal excitability). Different preprocessing transformations designed to improve the accuracy by which μ-alpha phase predicts excitability were also tested.

By fitting a sinusoid to the MEP amplitudes, sorted according to pre-stimulus EEG-phase, we found that excitability was highest during the early rising phase, at a significant delay with respect to the negative peak by on average 45° or 10 ms. The individual phase of highest excitability was consistent across study participants and unaffected by two different EEG-cleaning methods that utilize 64 channels to improve signal quality by compensating for individual noise level and channel covariance. Personalized transformations of the montage did not yield better prediction of excitability from μ-alpha phase.

The relationship between instantaneous phase of a brain oscillation and fluctuating cortical excitability appears to be more complex than previously hypothesized. In TMS of motor cortex, a standard surface Laplacian 5-channel EEG montage is effective in extracting a predictive signal and the phase corresponding to the highest excitability appears to be consistent between individuals. This is an encouraging result with respect to the clinical potential of therapeutic personalized brain interventions in the motor system. However, it remains to be investigated, whether similar results can be obtained for other brain areas and brain oscillations targeted with EEG and TMS.

* Corresponding authors at: Department of Neurology & Stroke, University of Tübingen, Germany.
E-mail addresses: christoph.zrenner@utoronto.ca (C. Zrenner), ulf.ziemann@uni-tuebingen.de (U. Ziemann).

https://doi.org/10.1016/j.neuroimage.2022.119805.
Received 21 August 2022; Received in revised form 30 November 2022; Accepted 9 December 2022
Available online 10 December 2022.

1. Introduction

Phase of sensorimotor μ-rhythm predicts corticospinal excitability, as indexed by the amplitude of motor evoked potentials (MEPs) when stimulating primary motor cortex with transcranial magnetic stimulation (TMS) (Bergmann et al., 2019; Hussain et al., 2019; Triesch et al., 2015; Zrenner et al., 2018). Sensorimotor μ-rhythm can be extracted effectively at rest using electroencephalography (EEG) with a 5-channel surface Laplacian montage (Hjorth, 1975; Kayser and Tenke, 2015) centered on EEG sensor C3 (nomenclature according to the 10–20 System of the International Federation of Clinical Neurophysiology (Jasper, 1958)). TMS during the negative peak of this 8–13 Hz oscillation results in larger MEPs on average, than during the positive peak (Schaworonkow et al., 2019; Stefanou et al., 2018; Triesch et al., 2015; Zrenner et al., 2018). Such EEG-defined excitability states can serve as "temporal targets" for brain-state-dependent TMS neuromodulation protocols. For example, repetitive stimulation with short bursts of TMS (3 pulses at 100 Hz) results in a long-term plasticity-like increase of excitability when the bursts are triggered at the negative peak of the μ-rhythm (corresponding to a high-excitability state) but not the positive peak (Zrenner et al., 2018). This investigation is motivated by the need to reliably detect phasic high-excitability states from EEG oscillation in order to develop more effective personalized therapeutic brain interventions following an information-based approach (Romei et al., 2016).

A crucial parameter in investigating the relationship between the phase of an EEG rhythm and instantaneous excitability is the spatial filter montage through which the relevant signal is extracted. Individualized montages designed to amplify the oscillation of interest (e.g., with spatial-spectral decomposition (Nikulin et al., 2011)) or designed to target a specific anatomical area (e.g., with beamforming, see (Gordon et al., 2021)) provide moderate benefit compared to a simple surface Laplacian centered on the EEG sensor of interest (Gordon et al., 2021; Schaworonkow et al., 2019). However, in these studies, only two distinct phase angles were compared, and the negative peak of the oscillation was hypothesized *a priori* to correspond to the high-excitability state. Other studies in the motor system investigating multiple phase angles have found the rising phase to also coincide with a state of high excitability using a C3 centered surface Laplacian (Bergmann et al., 2019; Wischnewski et al., 2022), or have found no consistent phase effect (Karabanov et al., 2021; Madsen et al., 2019), using various montages. Thus the assumption that the negative peak corresponds to the state with highest excitability requires further exploration.

The present study is designed to address three methodological aspects related to this assumption. First, we investigate when exactly a high-excitability state occurs with respect to a full cycle of the sensorimotor μ-rhythm. For this, we extract the sensorimotor μ-rhythm using a 5-channel C3-centered surface Laplacian montage (Hjorth, 1975) and a post hoc sorting approach similar to a previous study (Metsomaa et al., 2021). Specifically, we address whether the average phase of highest corticospinal excitability coincides with the negative peak of μ-rhythm. Second, we analyze whether the phase of highest excitability is consistent among participants for this montage. Finally, we test whether the result is affected by different preprocessing procedures designed to improve signal quality by participant-specific data-dependent transformations of the 5-channel C3-centered spatial filter: The first transformation aims to compensate for channel noise using the SOUND algorithm (Mutanen et al., 2018). The second transformation uses a beamformer approach to compensate for covariance between the channels (Haufe et al., 2014).

We treat EEG-defined brain-states as *temporal* targets that add a new dimension to the existing choice of *spatial* targets in the application of TMS which, we expect, will enable new and more effective treatments of neuropsychiatric disorders. In our view, the detection of localized phasic cortical excitability states is a critical challenge for the development of personalized neuromodulatory brain intervention protocols, informed by synaptic plasticity models such as spike-timing-dependent plasticity (Bell et al., 1997; Bi and Poo, 1998; Markram et al., 1997; Sjöström et al., 2001).

2. Materials and methods

2.1. Participants

60 right-handed participants (39 female, 21 male, mean ± SD age: 24.4 ± 3.7 years, age range: 18–36), with no history of neurological disease or substance use, were included in this study. We adhered to the current TMS safety guidelines of the International Federation of Clinical Neurophysiology (Rossi et al., 2021; Rossi et al., 2009). All participants gave written informed consent before measurements and tolerated the procedures without any adverse effects. The study protocol was approved by the ethics committee at the medical faculty of the University of Tübingen (protocol 716/2014BO2). 2 out of 60 participants were excluded from the analysis since channels from the 5-channel C3 centered surface Laplacian montage (C3, FC1, FC5, CP1, CP5) were determined to be noisy during automated preprocessing (see below for details). 6 of the remaining 58 participants were excluded because they did not complete 800 trials, yielding a dataset consisting of 52 study participants. Data from participants 1–8 has previously been reported in a similar analysis (Metsomaa et al., 2021).

2.2. Experimental set-up

Participants were seated in a comfortable chair and asked to keep their hands and arms relaxed. Single pulses of biphasic TMS were applied to the hand area of the left primary motor cortex using a figure-of-eight coil oriented such as to most effectively evoke muscle contractions in the right hand, corresponding to a direction of the major component of the induced electric field orthogonal to the precentral motor gyrus, from left posterolateral to right frontomedial. An EEG-compatible TMS stimulator was used (participants 1–9: MAG & More Research 100 with PMD70-pCool coil; participants 10–57: MagVenture R30 with MCF-B65 coil) with a stimulus intensity of 110% resting motor threshold. 64 channel EEG (participants 1–9: 126 channels) was recorded using a TMS-compatible sintered Ag/AgCl ring electrode cap system (EasyCap, Germany). Electromyography (EMG) was recorded using hydrogel foam electrodes (Kendall, Covidien/Medtronic, Ireland) in a bipolar belly-tendon montage from two muscles of the right hand (adductor pollicis brevis, and first dorsal interosseus). EEG and EMG were recorded using a 24 bit biosignal amplifier (NeurOne, Bittium, Finland) at 5 kHz in DC mode. A total of 800 pulses (participants 1–9: 1200 pulses) were triggered in a pre-programmed sequence with an inter-stimulus-interval of 2.25 s (participants 1–9: 2.0 s) and a jitter of ±0.25 s.

Data preprocessing

Data was processed using Mathworks Matlab (2021a). The first 800 trials and the same standard set of 64 EEG channels were loaded from all participants (more trials and channels were available for participants 1–9 but these were not considered in this study) to yield a homogenous dataset. EMG epochs were extracted surrounding the TMS stimuli in the period −100 ms to +100 ms (for the two EMG channels), and MEP amplitude was determined as the range of the EMG signal between +20 ms and +40 ms after each stimulus. A joint excitability index was computed for each trial from the MEP amplitudes from the two hand muscles by the following procedure: First, the two amplitudes were log-transformed thus reducing asymmetry in their distributions and reducing the relative magnitude of extreme values. A single value was then computed using principal component analysis and projecting the two amplitudes to the first principal component of the joint distribution. EEG epochs were extracted from the period between −604 ms and −5 ms (for the 64 EEG channels), detrended (linear fit, order 1) and downsampled to 1 kHz yielding a 600 ms pre-stimulus data window. Bad channels were automatically removed if the median range in that epoch and for that chan-

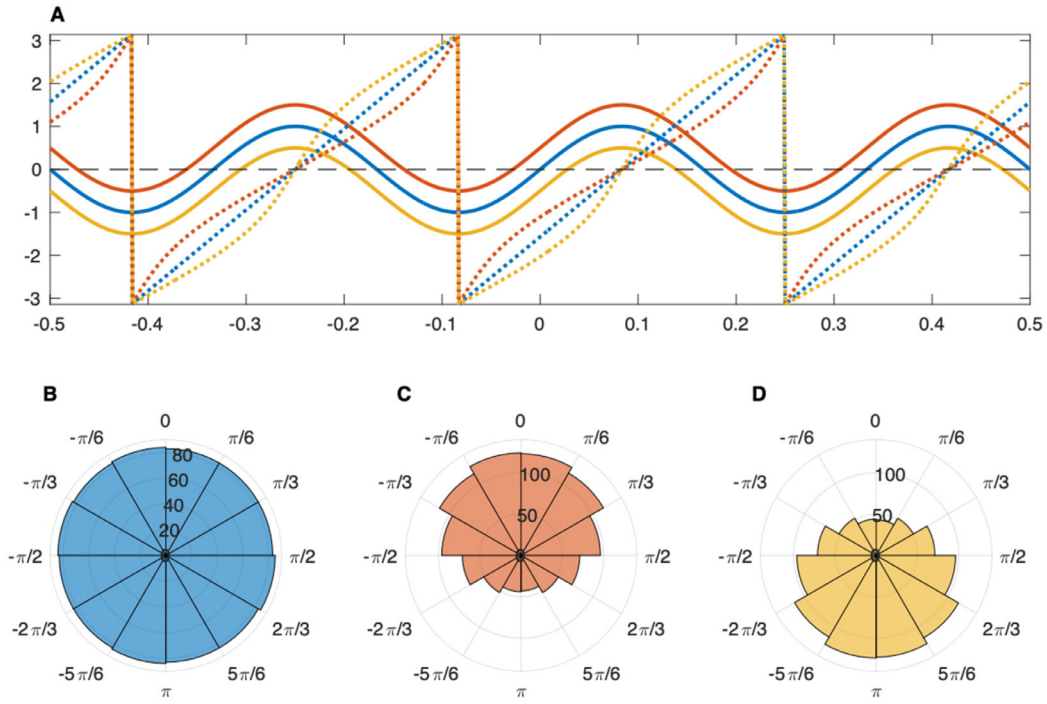

Fig. 1. Illustration of baseline shifts as a source of bias in phase estimation based on a Hilbert transformation. **(A)** Synthetic sinusoids (solid lines) with different zero offsets and corresponding instantaneous phase (dotted lines), derived from the angle of the Hilbert transformation. **(B–D)** The resulting phase distribution is homogenous for the zero-offset sinusoid (B), biased toward the positive peak in the case of an upward (offset greater than zero) shift of the baseline (D) and biased toward the negative peak in the case of a downward (offset smaller than zero) shift of the baseline (D).

nel exceeded 150 μV. This criterion was chosen to exclude channels exhibiting consistent slow drifts preceding the TMS pulse, which can cause problematic baseline shifts when included in the montage (Fig. 1). An average of 1.4 channels out of 64 were removed (median = 1, s. d. = 2.3, max. = 13). No bad trials were removed in order not to bias the results of the EEG cleaning transformations.

2.3. Signal quality optimization spatial filter transformations

The motivation behind investigating the effect of different spatial filter transformations designed to improve signal quality are twofold: Firstly, this allowed us to investigate whether the resulting phase of highest excitability was affected by procedures designed to clean the data and improve signal quality. Secondly, it allowed us to investigate whether different methods of extracting the signal of interest yield a more predictive (and in that sense 'better') signal. The specifics of the transformations are briefly described below.

The EEG datasets were preprocessed utilizing information from the complete 64-channel EEG channels to get an estimate of the cleaned signals from noiseless source localization (i.e., eliminating the sensor noise from the original data by subtracting cleaned source activity back to sensor level). Four different spatial filters were computed, all based on a surface Laplacian (Hjorth, 1975) centered on EEG sensor C3, and applied to the data to extract sensorimotor μ-rhythm. Namely: RAW·SL: Surface Laplacian transformation applied to raw data. SOUND·SL: surface Laplacian applied to SOUND cleaned data. RAW·BF: Beamforming as a forward spatial filter applied to raw data. SOUND·BF: Beamforming as a forward spatial filter applied to SOUND cleaned data.

2.3.1. SOUND cleaning spatial filter

The source-estimate-utilizing noise-discarding (SOUND) algorithm (Mutanen et al., 2018), uses the high dimensionality of EEG data to clean data from sources external to brain activity. SOUND consists of two conceptual steps: (1) noise estimation of each sensor by means of signals from the remaining sensors (2) cleaning of the whole EEG dataset according to the single sensor noise estimates. We briefly summarize the implementation of this procedure below.

The signal dataset can be written as:

$$\mathbf{Y} = \mathbf{Y}' + \mathbf{N} = \mathbf{LJ} + \mathbf{N} \tag{1}$$

where **Y** and **Y'** represent N × T matrices of the contaminated and the noise-free EEG (N channels) time signals (T samples), respectively, and **N** is the noise matrix with the same dimensions. Then, we can express **Y'** as the product of the leadfield matrix **L** and the source amplitude matrix **J**, where **J** is an array with dimension = S number of dipoles × T number of time samples.

To estimate **Y'** from **Y**, minimally noisy source estimates are extracted, and then used to estimate clean sensor signals, obtaining **Y'**.

Knowing the noise covariance matrix **Σ**, which denotes the spatial distribution of noise over sensor space, we can maximize signal-to-noise ratio (SNR) in the estimation of source currents **J**. Therefore, after multiplying (1) by $\mathbf{\Sigma}^{-\frac{1}{2}}$ to make the noise levels of unit size over all channels, **J** can be estimated by means of minimum-norm estimate (MNE):

$$\mathbf{J_e} = \mathbf{L'^T}\left(\mathbf{L'L'^T} + \lambda I\right)^{-1}\mathbf{Y'} \tag{2}$$

where **L'** represents the whitened leadfield and λ a regularization parameter that can be a priori selected

Assuming uncorrelated noise across the sensors, we estimate the standard deviation σ_n in each sensor. Starting with an initial guess for $\mathbf{\Sigma} = \mathrm{diag}(\sigma^2_{i1}, \ldots, \sigma_{iN})$, the sigma value estimations are iteratively updated by means of leave-one-channel-out cross-validation making use of (2) and then estimating the clean and noise signals within the left-out channel by (1). The final set $(\sigma^2{}_1, \ldots, \sigma^2{}_N)$ is employed to clean the measured data.

We calculate the cleaned version of our data as:

$$\mathbf{Y'} = \mathbf{L}(\mathbf{\Sigma}^{-1/2}\mathbf{L})^{\mathrm{T}}(\mathbf{\Sigma}^{-1/2}\mathbf{LL}^{\mathrm{T}}\mathbf{\Sigma}^{-1/2} + \lambda\mathbf{I})^{-1}\mathbf{\Sigma}^{-1/2}\mathbf{Y} = \mathbf{MY} \tag{3}$$

Table 1
Summary of the four spatial filter transformations. $\mathbf{W}_{SL}$ denotes the 5-channel surface Laplacian centered around C3. $\mathbf{M}$ and $\mathbf{w}_{BF}$ denote the SOUND cleaning matrix in Eq. (3) and the beamforming spatial filter in Eq. (5), respectively.

Filter	Description	Formula
RAW·SL	5-channel surface Laplacian applied to raw data, considering only channels C3, FC1, FC5, CP1, and CP5	$\mathbf{w}_{SL}$
SOUND·SL	5-channel surface Laplacian applied after 64-channel SOUND cleaning transformation	$\mathbf{M}^T\mathbf{w}_{SL}$
RAW·BF	64-channel beamforming-derived filter applied to raw data	$\mathbf{w}_{BF}(\mathbf{a})$
SOUND·BF	64-channel beamforming-derived filter applied after 64-channel SOUND cleaning transformation	$\mathbf{M}^T\mathbf{w}_{BF}(\mathbf{M}\mathbf{a}_{SL})$

with

$$\lambda = \lambda_0 \mathrm{trace}(\mathbf{\Sigma}^{-1/2}\mathbf{L}\mathbf{L}^T\mathbf{\Sigma}^{-1/2})/N$$

2.3.2. Beamformer as a backwards spatial filter

As outlined above, in Eq. (2), MNE was used in SOUND to clean the data via a source-modelling step. Additionally, we then used beamforming to estimate individualized spatial filters, which takes into account the variable EEG statistics across subjects, while still 'targeting' the same neuronal sources as C3-Hjorth does for idealistic noise free data. We emphasize that the application of beamforming presented here is conceptually distinct from its usage in EEG source estimation, but the theory and the mathematical properties of the estimated filter are the same, even though a head model is not required in this formulation.

When approaching source localization by means of a set of EEG data $\mathbf{Y}$ making use of beamforming (BF), the mapping from EEG signals to reconstructed source activity $\bar{\mathbf{s}}$, represented by the multi-sensor EEG topography a, can be captured by the spatial filter vector $\mathbf{w}_{BF}$:

$$\left(\mathbf{w}_{BF}\right)^T\mathbf{Y} = \bar{\mathbf{s}} \tag{4}$$

where the sensor filter $\mathbf{w}_{BF}$ is defined with the help of classic beamforming formulation as:

$$\mathbf{w}_{BF}(\mathbf{a}) = \left(\mathbf{C} + \lambda_{BF}\mathbf{I}\right)^{-1}\mathbf{a}\left(\mathbf{a}^T\left(\mathbf{C} + \lambda_{BF}\mathbf{I}\right)^{-1}\mathbf{a}\right)^{-1} \tag{5}$$

where $\mathbf{a}$ represents the sensor activity generated by a unitary dipole at the location of $\bar{\mathbf{s}}$ and $\mathbf{C}$ is the sensor covariance of the signal of interest estimated as a sample covariance.

While sensitivity to source activity is maximized in the target location, the optimal spatial filter maximizes orthogonality to the noise sources, suppressing them. In this way, we obtain estimated noiseless source activity time course $\bar{\mathbf{s}}$ by Eqs. (4) and (5).

To use beamforming as a sensor signal filter, we would need the topography representing the EEG spatial pattern for a predefined source distribution of interest. Here, the source distribution is not required to represent a single-dipole source activity (i.e., a lead-field matrix column), but any (fixed) source distribution predictive of the MEP amplitudes. Since a C3-centered surface Laplacian (SL) is known to be effective at predicting corticospinal excitability, we hypothesized that the respective topography estimated using noise-free EEG could serve as an educated guess for representing the relevant underlying source activity. By Haufe et al. (2014), the topography to which the spatial filter $\mathbf{w}_{SL}$ is maximally sensitized is obtained by:

$$\mathbf{a}_{SL} = \mathbf{\Sigma}_{\mathbf{Y}}\mathbf{w}_{SL}\mathbf{\Sigma}_{\bar{\mathbf{S}}}^{-1} \tag{6}$$

Here, we set the noise-free EEG covariance as $\mathbf{\Sigma}_{\mathbf{Y}} = \lambda^* + \mathbf{L}\mathbf{L}^T$, and $\mathbf{\Sigma}_{\bar{\mathbf{S}}} = (\mathbf{w}_{SL}^T\mathbf{\Sigma}_{\mathbf{Y}}\mathbf{w}_{SL})$, where λ is a regularization parameter unrelated to the λ used in Eq. (3). Thereby, we obtain the topography $\mathbf{a}_{SL}$ to be inserted in Eq. (5). The activation time-course of the underlying sources was then obtained by Eq. (4), and the output $\bar{\mathbf{s}}$ can be used to predict MEPs based on the phase estimate resulting from this signal.

2.3.3. Summary of derived spatial filter transformations

Four different types of spatial filters were derived using different combinations of the C3-centered surface Laplacian (SL), SOUND-cleaning by Eq. (3), and beamforming filtering by Eqs. (4) and (5). The spatial filter types are summarized in Table 1.

The surface Laplacian was applied with and without the SOUND cleaning. When using SOUND, the spatial filter $\mathbf{w}_{SL}$ can be merged with the SOUND correction matrix $\mathbf{M}$ in Eq. (3) to give the combined filter as $\mathbf{w}_{SL}\,\mathbf{M}^T$. In this way, the SOUND cleaning step does not need to be performed as a separate step.

Similarly, beamforming-based filter was also applied either with or without SOUND. When SOUND is applied, all underlying topographies, are transformed by operation Eq. (3). Thus, beamforming by Eq. (5) is computed using the transformed topography as $\mathbf{w}_{BF}(\mathbf{M}\mathbf{a}_{SL})$. As above, the two beamforming filter types are obtained as $\mathbf{w}_{BF}$ or $\mathbf{w}_{BF}\mathbf{M}^T$, for original or SOUND-cleaned data, respectively.

This resulted in the following spatial filter transformations:

2.4. Determination of the phase of highest excitability

We investigated the relationship between the phase of the μ-rhythm at the time of the stimulus and corticospinal excitability as follows: First, the signal of interest was extracted using the C3-centered 5-channel surface Laplacian montage directly or using one of the transformed spatial filters, yielding four different EEG signals for the window of data preceding each stimulus. Second, the phase at the time of the stimulus was estimated for each trial using the PHASTIMATE function as implemented in Matlab (Zrenner et al., 2020b) using standard parameters (sample rate 1 kHz; window size 600 ms; windowed FIR filter order 128 with pass-band 9–13 Hz; edge removal 64 samples; autoregressive model order 30) and configuring the forward prediction to bridge both the filter edge and the 5ms offset to the timepoint of interest. These settings were used for each participant, as individualized parameters only improve estimator accuracy moderately (Zrenner et al., 2020b) and not every participant exhibited a clear alpha peak in the spectral analysis (see below for details on the spectral estimation).

Then, a sinusoidal, circular-to-linear regression was computed between the pre-stimulus phase estimates and the excitability index derived from post-stimulus MEP amplitudes, separately for the phase estimates resulting after application of the four different spatial filters, yielding a p-value (against the null hypothesis of a constant value fit with no effect of phase) and an R^2-value as a goodness-of-fit measure for each regression fit. The phase corresponding to maximum excitability (peak of the fitted sine wave) was determined for each transformation. Note that this analysis assumes a sinusoidal model, which may be a simplification given the arch-like asymmetric nature of the μ-rhythm (Schaworonkow and Nikulin, 2019) associated with a relatively short duration of the high-excitability phase (Bergmann et al., 2019).

The phase-estimation method used in this study, PHASTIMATE (Zrenner et al., 2020b), is based on the Hilbert transform. As such, artifacts such as line noise, or drifts can bias the estimate (see Fig. 1 for an illustration), but also the asymmetric nature of the μ-rhythm oscillation can lead to inhomogeneities in the distribution of phase estimates. To control for the possibility of bias in the phase estimation algorithm affecting the results, we also perform the regression analysis with data where the EMG amplitudes are randomly shuffled among the trials.

2.5. Spectral estimation and circular statistics

Power spectra were computed from 1 s long pre-stimulus data windows (800 trials) using Hanning-windowed FFT. The 1/f aperiodic

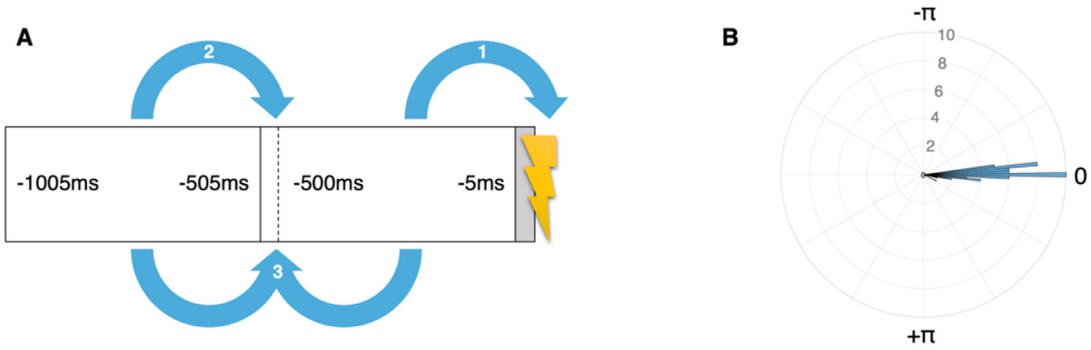

Fig. 2. Validation of phase estimation method. **(A)** In addition to the causal estimate of phase at the time of the stimulus (1), phase is also estimated at an earlier time with the same algorithm (2), that is not affected by the stimulus artifact and where the estimate can be compared with a standard phase determination using data before and after the time of interest (3). **(B)** Histogram showing the average difference by-participant between the causal and standard estimate (mean phase difference < 0.1°).

component of the spectrum was estimated using the IRASA (Wen and Liu, 2016) method with 18 factors between 1.1 and 2.9 (excluding 2.0) and subtracted from the full spectrum yielding the periodic component, which can be considered the SNR of the oscillation at a given frequency. We follow the cosine convention for angular data where 0 degrees corresponds to the positive peak of the oscillation, $-\pi/2$ (−90°) to the rising phase, $+\pi/2$ (+90°) to the falling phase, etc. Circular statistics were performed using the Circular Statistics Toolbox for MATLAB (Berens, 2009).

3. Results

3.1. Phase estimation accuracy

Due to the stimulus artifact affecting the signal after the TMS pulse, it is not possible to assess the phase at the time of the stimulus with standard signal processing methods. Therefore, in order to assess the accuracy of the causal phase estimation method implemented in the PHASTIMATE script (Zrenner et al., 2020b), we used an earlier window of data not affected by a stimulus artifact (see Fig. 2). This allowed us to compare the causal (preceding data only) phase estimate with a standard symmetrical estimate to validate that there was no systematic bias. The mean circular difference between the estimates was <0.1°.

3.2. Illustration of procedure to determine high-excitability state

A representative example dataset illustrating the procedure is shown in Figs. 3 and 4. This serves to visualize the processing pipeline and shows the type of data obtained at the single participant and single trial level (Fig. 4). With regard to the spatial filter transformations (Fig. 3), note that the power spectral densities estimated from the pre-stimulus windows are similar regardless of the spatial filter used to extract the signal (Fig. 3A), showing a peak at 11 Hz and three harmonics, indicating a strong sensorimotor μ-rhythm (see also the inset of Fig. 4 for a phase-locked depiction of the oscillation). The sinusoidal regression fit and the phase of peak excitability, determined as the maximum of the fitted sine, is also similar for all four spatial filters at the early rising phase, around −140° (Fig. 4).

3.3. High-excitability state group results

Next, we analyzed the distribution across all 52 participants of the phase corresponding to the state of highest excitability, which differs significantly from the uniform distribution for all four cleaning transformations (RAW·SL: $p = 5 \times 10^{-8}$; SOUND·SL: $p = 1 \times 10^{-5}$; RAW·BF: $p = 2 \times 10^{-5}$; SOUND·BF: $p = 4 \times 10^{-5}$). The average phase angle is in the early rising phase (for the four filters respectively: circular mean = −124°, −123°, −129°, −129°; circular median = −137°, −134°, −133°, −126°) and the 99% confidence interval does not encompass the negative peak of the oscillation (−180°), which was previously assumed to correspond to the phase angle of highest excitability, for all four cleaning transformations (circular *t*-test, $p < 0.001$). The distribution for the raw SL filter is shown in Fig. 5A.

As a control, we verified the distribution of phases across trials. The overall distribution of phase estimates from all 52 participants (800 trials per participant) is biased toward the rising and falling phase (Fig. 5B), and the Rayleigh test for non-uniformity reaches $p < 0.05$ in at least one of the four spatial filters for 3 out of 52 study participants. However, this does not appear to significantly bias the sinusoidal regression in a shuffled data control (100 repetitions), which does not differ significantly from a uniform distribution (Fig. 5C).

3.4. Consistency of high-excitability phase across participants

To exclude the influence of noisy results from datasets where no significant relationship between pre-stimulus phase and corticospinal excitability could be found or where non-uniformity of the phase estimates might bias the fit, a subgroup analysis was performed, by applying the following criteria: For all subsequent analysis, the 3/52 participants where the distribution of phase estimates differed from uniformity as described above, were excluded. Further, data was only included in the analysis where the regression fit reached a significance threshold individually. This was performed in two different ways: (1) inclusion by subject, considering only subjects where at least one of the cleaning transformations led to a significant sinusoidal regression fit at a p-value threshold of 0.05, but then including all data from each subject (this was the case for 24/49 participants), see Fig. 6A; (2) inclusion by cleaning transformation, considering only datasets with significant regression fits at a p-value threshold of 0.05 (this was the case for between 12 and 16 datasets depending on the transformation), see Fig. 6B.

As can be seen in Fig. 6, the average phase corresponding to highest corticospinal excitability is found consistently at the early rising phase of the sensorimotor μ-rhythm also for these subgroups. The circular mean angle of highest excitability was, for the respective filters, −134°, −141°, −140°, −134°, with subgroups selected by participant and −140°, −151°, −133°, −132°, for the subgroups selected by transformation. The mean angle differs significantly from the negative peak of the oscillation for all four cleaning transformations in both subgroups (circular t-test, alpha = 0.05). No significant difference could be detected in the resulting phase angles, when comparing them pairwise for all cleaning transformations (parametric Watson-Williams multi-sample test, see (Berens, 2009)) within both the by-subject and by-transformation subgroups.

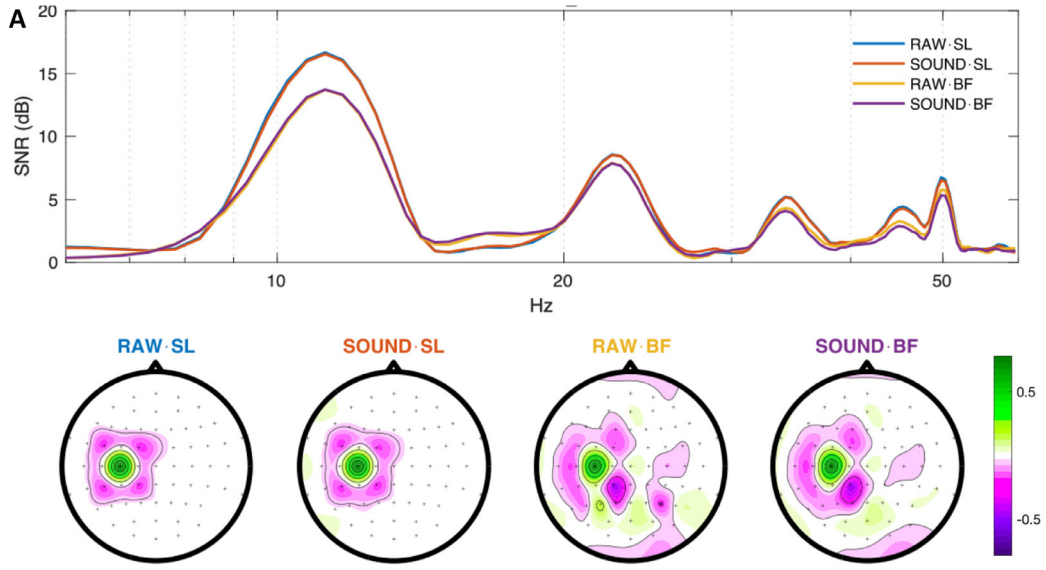

Fig. 3. Spatial filter transformations based on a C3-centered 5-channel surface Laplacian (SL). Data from a representative study participant. **(A)** Spectral analysis of the resulting signal from each transformation, showing signal-to-noise ratio (SNR) after removal of aperiodic 1/f component of spectrum using the IRASA method. 11.5 Hz peak and 3 harmonic frequencies are visible corresponding to sensorimotor μ-rhythm. **(B)** Topography of spatial filters weights corresponding to each of the four transformations. RAW·SL/SOUND·SL: Surface Laplacian transformation applied to raw data and to SOUND cleaned data, respectively. RAW·BF/SOUND·BF: Beamforming as a forward spatial filter applied to raw data and SOUND cleaned data, respectively.

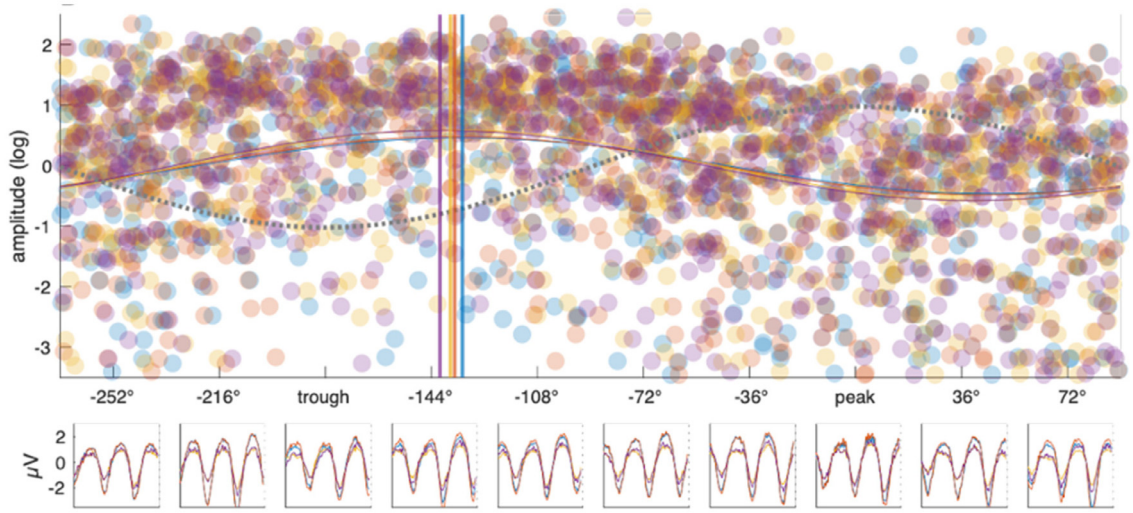

Fig. 4. Example dataset from a representative study participant consisting of 800 single TMS pulses to the hand area of primary motor cortex while recording EEG. Scatter plot of phase, determined post-hoc from pre-stimulus EEG, vs. log-transformed MEP amplitude. Phase is estimated separately for each spatial filter (color coding as in panel A). The sinusoidal regression fit is shown (solid curves) for each transformed data and the peaks are also indicated by the vertical lines. Dotted sinusoid illustrates the corresponding μ-rhythm phase. Insets: Average pre-stimulus EEG shown after discretizing data into 10 phase bins, below panel.

3.5. Influence of data cleaning transformations

Since the choice of cleaning transformation did not significantly impact the average phase of highest excitability, we investigated whether the cleaning transformations differed with respect to how well phase predicted MEP amplitude in the regression analysis. A qualitative analysis of the resulting significance level and variance explained is shown in Fig. 7. The proportion of participants reaching individual significance in the sinusoidal regression fit at a p-value threshold of 0.1 was 35% for the 5-channel surface Laplacian (33% when combined with 64-channel SOUND cleaning), and 37% for the backwards beamforming-based method (29% when combined with SOUND).

In summary, the phase angle of sensorimotor μ-rhythm extracted with a montage centered on EEG sensor C3 corresponding to the highest corticospinal excitability falls on the early rising phase, about 45° after the trough of the oscillation and this result is consistent between participants and robust under various spatial filter transformations designed to improve signal quality. However, the predictive power of the EEG signal from a 5-channel C3-centered Hjorth-style SL montage is not or only marginally improved by the specific SOUND and/or beamforming-based cleaning transformations tested here.

3.6. Offset to the negative peak

For 38 of 52 participants, a single peak frequency in the SNR spectrum could be determined between 8.5 and 14 Hz (the peak frequency of average SNR was 11.25 Hz). For these participants, it was also possible to convert the offset between the negative peak and the time of the

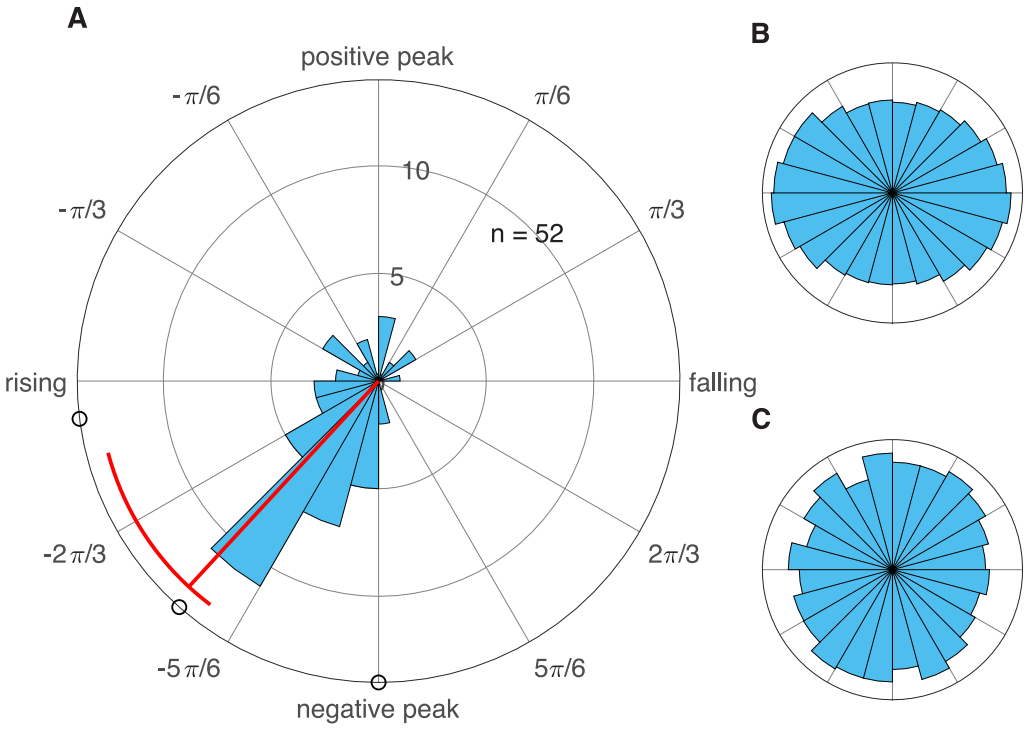

Fig. 5. **(A)** Distribution of phase of maximum corticospinal excitability of sensorimotor μ-rhythm extracted using a C3-centered 5-channel surface Laplacian for all 52 participants, according to circular-to-linear sinusoidal regression between phase and MEP size (800 trials per participant). Circular median phase angle (−134°) and 95% confidence interval of circular mean (−143° to −105°) indicated. Magnitude is number of participants. Note that the median is more robust to outliers which is why the confidence interval of the mean appears skewed. **(B)** Normalized overall distribution of phase estimates for all 52 participants. **(C)** Normalized distribution of phase angle of highest corticospinal excitability for all data with MEP amplitudes randomly shuffled (100 repetitions).

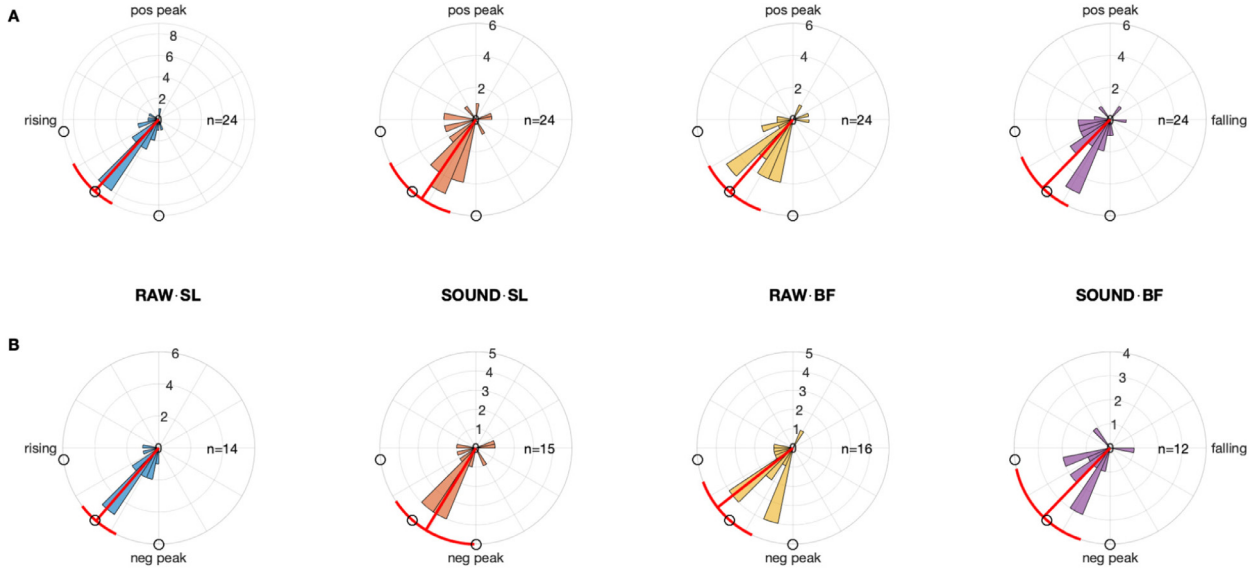

Fig. 6. Distribution of peak excitability phase across subjects, showing the circular mean ±95% confidence intervals (red line and segment) of μ-rhythm extracted with different EEG spatial filters: 5-channel C3 centered surface Laplacian (SL) of raw data and after SOUND transformation, beamformer (BF) transformation of sensitivity profile on raw and on SOUND transformed data. Magnitude is number of participants. **(A)** Data selection by participant (excluding participants where the sinusoidal regression did not reach a $p < 0.05$ significance threshold for any of the spatial filter transformations). **(B)** Data selection by transformation, considering all sinusoidal fits reaching a $p < 0.05$ significance threshold (this leads to unequal sample sizes). For illustration, the timing of the three pulses of a 100 Hz TMS triplet, if it were triggered with the first pulse of the triplet at the negative peak, as in previous studies to induce plasticity, is indicated for a 10 Hz μ-rhythm frequency (circle mark).

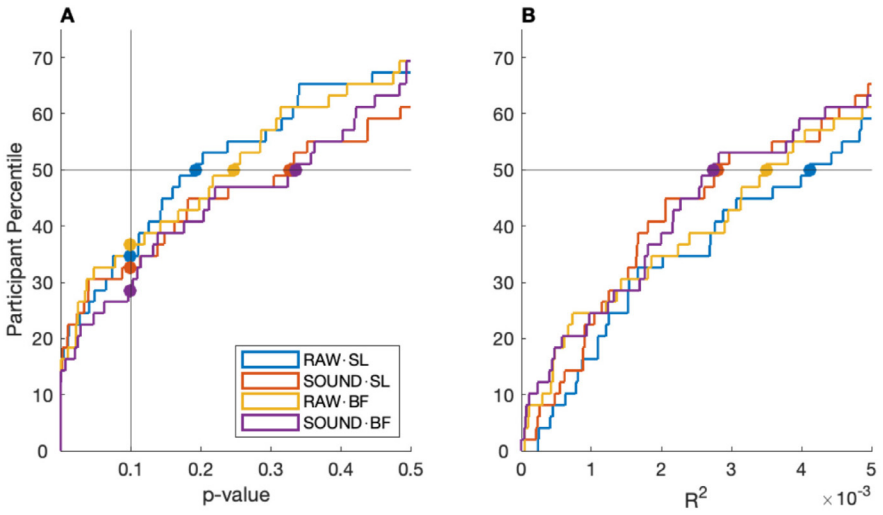

Fig. 7. Comparison of the results of circular to linear regression fitting of a sinusoid to predict MEP amplitude (log-transformed to reduce asymmetry of the distribution) from post-hoc estimated EEG phase at the time of the TMS pulse recorded from a montage centered on EEG sensor C3 after four different data cleaning transformations. 49/52 participants are included in this analysis, 3 participants with inhomogeneous phase distributions (Rayleigh test for non-uniformity $p < 0.05$ in any of the transformations) were excluded. **(A)** Cumulative histogram of p-value of the sinusoid regression fit in comparison to the alternative assumption of no phase effect. Median p-value indicated (50th percentile) for each cleaning transformation, and proportion of participants reaching an individual significance level of $p < 0.1$ for the given EEG cleaning transformation. **(B)** Cumulative histogram of proportion of variance of MEP amplitudes explained by the regression model (median R^2-value indicated for each cleaning transformation).

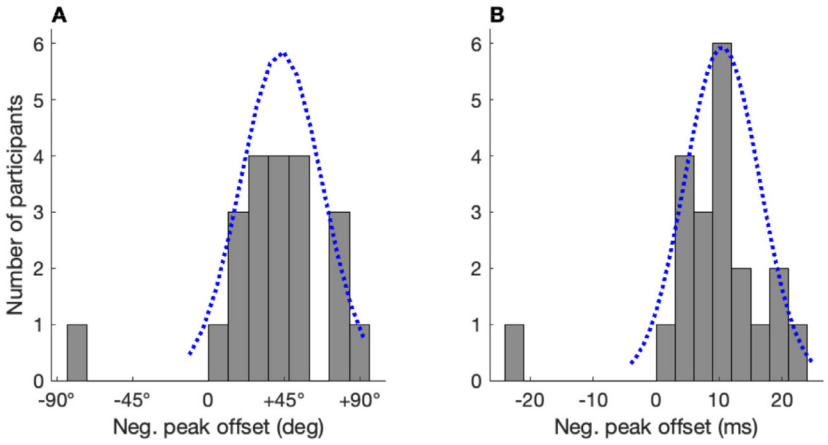

Fig. 8. Offset of highest corticospinal excitability relative to the negative peak. (**A**) Data shown in cycles and (**B**) in milliseconds. 21 participants were included in this analysis, having a significant fit in any of the cleaning transformations, and having an individual alpha in the range between 8.5 and 14.0 Hz. Fitted Gaussian indicated (dotted blue curves).

highest excitability from cycles to time (radian to millisecond). 23 of the 38 participants in this subgroup also satisfy the phase homogeneity and regression fit significance thresholds used for the analysis above and the distribution of the offset to the negative peak is shown for this group (Fig. 8). Excluding 1 outlier, the resulting distribution of 22 participants had a circular mean of 43° (circular deviation: 23°) and 10 ms (standard deviation: 6 ms) after converting the individual offsets relative to the negative peak from cycles to time.

4. Discussion

4.1. Summary

This post-hoc analysis of open-loop high-density EEG and TMS datasets from 52 healthy participants enabled the data-driven investigation into the relationship between the phase of sensorimotor 9–13 Hz μ-rhythm and corticospinal excitability. Individual significance testing for a sinusoidal fit yielded a p-value < 0.05 in 14/49 (29%) of study participants. The median phase of highest excitability according to the result of the regression (whether significant or not) was at −134° (in cosine convention, relative to positive peak). This result provides strong evidence ($p < 0.001$) that the phase of highest excitability does not coincide precisely with the negative peak of the μ-rhythm, but instead occurs later by approx. ⅛ of a cycle, or about 10 ms.

4.2. Neurophysiology

This offset from the negative peak is meaningful as it breaks the equivalence between phase and signal magnitude as predictors of excitability (Schalk, 2015) (during the early rising phase and during the late falling phase the absolute voltage value is the same, but excitability is different), demonstrating the relative timing within the activity cycle is decisive. The negative peak in a surface Laplacian montage corresponds to inward currents (scalp to brain) and maximal currents were thought to correspond to maximal excitability because excitatory postsynaptic potentials (EPSPs) at the apical dendrites of radially oriented pyramidal cells are a major contributor to such currents (Zschocke and Hansen, 2011) and also reduce the additional excitatory input required to reach the action potential threshold. A similar relationship between the phase of local field potential oscillations and spike rate of neurons in sensorimotor cortex was found experimentally in primates (Haegens et al., 2011).

However, the EEG montage used in this study is most sensitive to radially oriented dipoles underlying sensor C3, which is typically located over the postcentral gyrus (somatosensory cortex). Whereas the crown of post-central gyrus is a strong generator of sensorimotor μ-rhythm, the eventual target cells of stimulation with TMS are the upper motoneurons in the hand knob area of primary motor cortex. These cells are located in the anterior wall of the central sulcus (Geyer et al., 1996). They are oriented tangentially to the scalp and a surface Laplacian EEG montage

is not sensitive to their activity. Therefore, we may be measuring activity originating predominantly from primary sensory cortex (S1) while stimulating primary motor cortex (M1) transsynaptically through various interneuron pathways including through S1 and premotor areas (for reviews: (Amassian et al., 1987; Di Lazzaro et al., 2008; Siebner et al., 2022; Ziemann, 2020)). This suggests that the relationship between μ-rhythm phase and MEP amplitude is influenced by the functional connectivity between S1 and M1, a pathway that has been characterized anatomically (DeFelipe et al., 1986) and with paired associative stimulation (Wolters et al., 2005), and the estimated S1-M1 pathway conduction time of ~7 ms (Wolters et al., 2005) may be a partial explanation for the observed phase offset from the negative peak (Zrenner et al., 2022).

Biophysical modeling studies may also shed some light on the relationship between oscillatory phase and spiking activity, especially the combination of models using detailed electrical field modelling (Alekseichuk et al., 2019) which determines the effective electrical field for each spatial position in a detailed 3D human head model, with functional network models of cortical responses to transcranial stimulation (Rusu et al., 2014; Schaworonkow and Triesch, 2018). Different cell types may have a different TMS activation threshold due to their size, morphology and laminar position, as well a different preferred spiking activity window relative to the phase of an ongoing oscillation (Shirinpour et al., 2021; Zhang and Frohlich, 2022).

Insights from modelling studies are especially relevant in future development of effective neuromodulatory repetitive stimulation protocols, since the parameter space of all possible intervention protocols is too large to be explored empirically, with conventional parameters of target location, stimulation intensity, pulse frequency and pattern, and number of pulses now additionally multiplexed with features related to the ongoing activity, such as oscillatory phase and amplitude.

4.3. Personalization of the EEG montage

Whereas this study was performed as a post-hoc trial sorting analysis of “open-loop” stimulation, we nevertheless purposefully did not preprocess the data with traditional cleaning methods such as ICA, in order for the findings to be directly applicable to a “closed-loop” setting. Instead, we compared the standard 5-channel surface Laplacian to three different spatial filter transformations that depended on the individual channel noise and covariance (accounting for all 64 channels). These transformations are designed to optimize signal quality using different techniques and they can also be applied in real-time in principle. The individualized transformations did not affect the resulting phase of maximum excitability. The question remains why these transformation did not improve the predictive power compared to the standard 5-channel montage.

One explanation may be that the sensorimotor μ-rhythm (recorded at rest with eyes open) is already a prominent oscillation without further signal conditioning. A standard 5-channel surface Laplacian may then extract a signal with a sufficient SNR in most participants and additional optimizations of the spatial filter only have a marginal benefit. There may also be advantages to sparse spatial filters that make use of only a small number of informative channels, and are unaffected by fluctuating noise levels in the other channels. Since we did not pre-clean the data and used short epochs between TMS pulses that were affected by slow decay artifacts and eye blinks, our covariance matrix estimate was likely noisy, which would negatively impact the resulting SOUND and beamforming filters. In summary, the personalized optimizations of the spatial EEG filter, that we tested in this study, did not appear to yield relevant benefit in extracting sensorimotor μ-rhythm, however, they may have a role in extracting less prominent oscillations in other cortical networks.

4.4. Generalizability of the result

Given that the EEG caps are all placed slightly differently in relation to the individual anatomy, and the coil position was also not targeted anatomically, the high degree of consistency of the phase angle of the μ-rhythm corresponding to the highest corticospinal excitability between different subjects and the invariance to data transformations is notable. However, it remains to be explored whether the phase of highest excitability is also offset from the negative peak in other brain oscillations, that are relevant for EEG-triggered TMS, such as dorsomedial prefrontal theta (Gordon et al., 2021) or dorsolateral prefrontal alpha (Zrenner et al., 2020a).

Another question is whether the −135° phase angle also corresponds to a state of high cortical excitability in those study participants, where a relationship to MEP amplitude cannot be demonstrated. This would be the case if the contribution of *spinal* circuits to the variability of MEP amplitudes dominates so that the influence of *cortical* excitability fluctuations is masked. For example, the phase of ongoing beta oscillations has been found to influence MEP amplitude at a spinal, but not cortical level in a study with a similar design to this experiment, but investigating beta oscillations (van Elswijk et al., 2010). This scenario could also explain why some participants don’t show a μ-oscillation phase effect on MEP amplitude, even though a high SNR oscillation can be extracted. An alternative possibility is that spatial mixing with unrelated oscillations such as occipital alpha prevents accurate μ-rhythm phase estimation in some persons. Finally, even if the measured μ-rhythm is generated by post-synaptic potentials in postcentral gyrus, this somatosensory activity is not necessarily reliably related to the excitability of primary motor cortex.

4.5. Implications for neuromodulation and therapeutic applications

The findings herein have implications for how high-frequency TMS bursts should be aligned with the phase of highest excitability if the goal is to maximize induced plasticity. Retrospectively, the 100 Hz triplet stimulation used in previous studies (Desideri et al., 2018; Zrenner et al., 2018) that was triggered by the trough of the oscillation was in fact, and perhaps fortuitously, centered around the phase of highest excitability (see Figs. 5 and 6). On the other hand, the repetitive single pulse stimulation used previously in a trough-triggered 1 Hz protocol (Baur et al., 2020) was in fact applied about 10 ms before the instant of average highest excitability. It remains an open question which stimulus parameters (number of pulses, frequency, intensity) at which phase optimally result in the desired neuromodulatory outcome.

A positive implication of this study for therapeutic brain-state dependent stimulation is that, at least in the motor system, a fixed 5-channel EEG montage and a fixed target phase are sufficient to target a state of high corticospinal excitability, with little or no detriment as compared to a 64-channel individually optimized montage and phase. This is of considerable practical significance, as it makes personalized EEG-triggered TMS protocols feasible in a clinical context.

4.6. Limitations

This study has some limitations: Firstly, our circular to linear regression analysis assumes a sinusoidal relationship between sensorimotor rhythm phase and corticospinal excitability, i.e., a single region of highest excitability and a corresponding symmetric single region of lowest excitability at the opposite phase angle. The advantage of this model is its simplicity, enabling a robust fit of 800 trials in spite of the high variability of MEP amplitude as an index of cortical excitability. Nevertheless, a further investigation of the actual relationship between phase and excitability, which may well not be symmetric, seems warranted (e.g., using gaussian process regression) and could yield a better model fit. Specifically, there is evidence that the period of high-excitability is relatively shorter, as proposed by a pulsed facilitation

model (Bergmann et al., 2019). Note also that the circular regression approach simultaneously fits the high-excitability and low-excitability (facilitation and inhibition) portion of the cycle and assumes a constant relationship, even though these may due to separable underlying neurophysiological mechanisms and may differ from trial to trial.

Secondly, we did not try to optimize the spatial filter used to extract the oscillation of interest, but only tested some transformations designed to clean the data. Whereas the result is robust for the chosen EEG montage, it is possible that a different result could be derived from an EEG montage other than a C3-centered surface Laplacian (Madsen et al., 2019), and this warranted further investigation. We also only considered the alpha frequency band from 9–13 Hz and we included study participants that did not have a clear spectral peak in this range, as we did not wish to pre-select study participants.

Our analysis is also limited to a relationship between phase of an alpha-band oscillation and excitability. Other predictors (such as different frequency bands, oscillatory amplitude, network connectivity, etc. (Hussain et al., 2019; Metsomaa et al., 2021; Thies et al., 2018)) are not included in our model. We also did not compensate for slow drifts in average MEP amplitude during the experiment (Metsomaa et al., 2021) which was seen in many of the participants. Finally, causal phase estimation may be possible with a higher accuracy using estimation algorithms that incorporate a state space model (Wodeyar et al., 2021), which may enable detection of a phase relationship in a larger proportion of participants.

4.7. Outlook

The neurophysiology of the relationship between μ-rhythm phase and high vs. low corticospinal excitability is not as simple (negative peak vs. positive peak) as we and others previously assumed. On the other hand, the finding that a 5-channel EEG recording at standard sensor locations can detect a specific brain-state using a fixed phase target and without the need for individual calibration and sophisticated data-preprocessing is an encouraging finding for future clinical applications. Detecting the excitability of cortical areas targeted by TMS based on the phase of a single oscillation is an important foundation for future applications that incorporate the relationship between multiple oscillations to enable personalized pathway-specific neuromodulation (Stefanou et al., 2018) and a benchmark for brain-state estimation methods that go beyond phase (Metsomaa et al., 2021). Beyond the neurophysiological findings, we hope that this dataset will be useful to facilitate addressing some of the remaining methodological optimizations (e.g., online data cleaning, signal extraction by spatial filter personalization, including statistical models for the interpretation of evoked responses, as well as improved phase estimation algorithms) for personalized brain stimulation to become a standard method.

Data availability statement

Data and code is available on request from the authors.

Disclosures

C. Z. declares an interest in sync2brain GmbH (Tübingen, German), a spin-off start-up commercializing technology for real-time EEG analysis.

Data and code availability statement

The source code of the scripts used for the analysis are available from the lab's GitHub repository: http://www.github.com/bnplab/highx

The data are available upon request. There is no consent from the study participants to make the data publicly available.

Data Availability

Data will be made available on request.

Credit authorship contribution statement

Christoph Zrenner: Conceptualization, Methodology, Software, Investigation, Formal analysis, Writing – original draft, Writing – review & editing, Visualization, Supervision, Funding acquisition. **Gábor Kozák:** Methodology, Investigation, Writing – review & editing. **Natalie Schaworonkow:** Conceptualization, Methodology, Software, Investigation, Writing – review & editing. **Johanna Metsomaa:** Conceptualization, Methodology, Software, Writing – review & editing. **David Baur:** Investigation, Writing – review & editing. **David Vetter:** Investigation, Writing – review & editing. **Daniel M. Blumberger:** Writing – review & editing. **Ulf Ziemann:** Conceptualization, Investigation, Writing – original draft, Writing – review & editing, Supervision, Funding acquisition. **Paolo Belardinelli:** Conceptualization, Methodology, Software, Investigation, Formal analysis, Writing – original draft, Writing – review & editing.

Acknowledgments

This work was supported by an EXIST Transfer of Research grant by the German Federal Ministry for Economic Affairs and Energy (NEUROSYNC) [grant number 03EFJBW169], by the European Research Council (ERC Synergy) under the European Union's Horizon 2020 research and innovation program (ConnectToBrain) [grant number 810377], by the KAUTE Foundation, and by the Emil Aaltonen Foundation. DMB receives research support from the Canadian Institutes of Health Research (CIHR), National Institutes of Health (NIH), Brain Canada Foundation and the Temerty Family through the CAMH Foundation and the Campbell Family Research Institute. We acknowledge support by the Open Access Publishing Fund of the University of Tübingen.

References

Alekseichuk, I., Mantell, K., Shirinpour, S., Opitz, A., 2019. Comparative modeling of transcranial magnetic and electric stimulation in mouse, monkey, and human. Neuroimage 194, 136–148.

Amassian, V., Stewart, M., Quirk, G., Rosenthal, J., 1987. Physiological basis of motor effects of a transient stimulus to cerebral cortex. Neurosurgery 20, 74–93.

Baur, D., Galevska, D., Hussain, S., Cohen, L.G., Ziemann, U., Zrenner, C., 2020. Induction of LTD-like corticospinal plasticity by low-frequency rTMS depends on pre-stimulus phase of sensorimotor μ-rhythm. Brain Stimul. 13, 1580–1587.

Bell, C.C., Han, V.Z., Sugawara, Y., Grant, K., 1997. Synaptic plasticity in a cerebellum-like structure depends on temporal order. Nature 387, 278–281.

Berens, P., 2009. CircStat: a MATLAB toolbox for circular statistics. J. Stat. Softw. 31, 1–21.

Bergmann, T.O., Lieb, A., Zrenner, C., Ziemann, U., 2019. Pulsed facilitation of corticospinal excitability by the sensorimotor μ-alpha rhythm. J. Neurosci. 39, 10034–10043.

Bi, G.-q., Poo, M.-m., 1998. Synaptic modifications in cultured hippocampal neurons: dependence on spike timing, synaptic strength, and postsynaptic cell type. J. Neurosci. 18, 10464–10472.

DeFelipe, J., Conley, M., Jones, E., 1986. Long-range focal collateralization of axons arising from corticocortical cells in monkey sensory-motor cortex. J. Neurosci. 6, 3749–3766.

Desideri, D., Zrenner, C., Gordon, P.C., Ziemann, U., Belardinelli, P., 2018. Nil effects of μ-rhythm phase-dependent burst-rTMS on cortical excitability in humans: a resting-state EEG and TMS-EEG study. PLoS One 13, e0208747.

Di Lazzaro, V., Ziemann, U., Lemon, R.N., 2008. State of the art: physiology of transcranial motor cortex stimulation. Brain Stimul. 1, 345–362.

Geyer, S., Ledberg, A., Schleicher, A., Kinomura, S., Schormann, T., Bürgel, U., Klingberg, T., Larsson, J., Zilles, K., Roland, P.E., 1996. Two different areas within the primary motor cortex of man. Nature 382, 805–807.

Gordon, P.C., Dörre, S., Belardinelli, P., Stenroos, M., Zrenner, B., Ziemann, U., Zrenner, C., 2021. Prefrontal theta-phase synchronized brain stimulation with real-time EEG-triggered TMS. Front. Hum. Neurosci. 335, 691821.

Haegens, S., Nácher, V., Luna, R., Romo, R., Jensen, O., 2011. α-Oscillations in the monkey sensorimotor network influence discrimination performance by rhythmical inhibition of neuronal spiking. Proc. Nat. Acad. Sci. 108, 19377–19382.

Haufe, S., Meinecke, F., Görgen, K., Dähne, S., Haynes, J.-D., Blankertz, B., Bießmann, F., 2014. On the interpretation of weight vectors of linear models in multivariate neuroimaging. Neuroimage 87, 96–110.
Hjorth, B., 1975. An on-line transformation of EEG scalp potentials into orthogonal source derivations. Electroencephalogr. Clin. Neurophysiol. 39, 526–530.
Hussain, S.J., Claudino, L., Bönstrup, M., Norato, G., Cruciani, G., Thompson, R., Zrenner, C., Ziemann, U., Buch, E., Cohen, L.G., 2019. Sensorimotor oscillatory phase–power interaction gates resting human corticospinal output. Cereb. Cortex 29, 3766–3777.
Jasper, H.H., 1958. The ten-twenty electrode system of the international federation. Electroencephalogr. Clin. Neurophysiol. 10, 370–375.
Karabanov, A.N., Madsen, K.H., Krohne, L.G., Siebner, H.R., 2021. Does pericentral mu-rhythm "power" corticomotor excitability? A matter of EEG perspective. Brain Stimul. 14, 713–722.
Kayser, J., Tenke, C.E., 2015. On the benefits of using surface Laplacian (current source density) methodology in electrophysiology. Int. J. Psychophysiol. Off. J. Int. Organ. Psychophysiol. 97, 171.
Madsen, K.H., Karabanov, A.N., Krohne, L.G., Safeldt, M.G., Tomasevic, L., Siebner, H.R., 2019. No trace of phase: corticomotor excitability is not tuned by phase of pericentral mu-rhythm. Brain Stimul. 12, 1261–1270.
Markram, H., Lübke, J., Frotscher, M., Sakmann, B., 1997. Regulation of synaptic efficacy by coincidence of postsynaptic APs and EPSPs. Science 275 (5297), 213–215.
Metsomaa, J., Belardinelli, P., Ermolova, M., Ziemann, U., Zrenner, C., 2021. Causal decoding of individual cortical excitability states. Neuroimage, 118652.
Mutanen, T.P., Metsomaa, J., Liljander, S., Ilmoniemi, R.J., 2018. Automatic and robust noise suppression in EEG and MEG: the SOUND algorithm. Neuroimage 166, 135–151.
Nikulin, V.V., Nolte, G., Curio, G., 2011. A novel method for reliable and fast extraction of neuronal EEG/MEG oscillations on the basis of spatio-spectral decomposition. Neuroimage 55, 1528–1535.
Romei, V., Thut, G., Silvanto, J., 2016. Information-based approaches of noninvasive transcranial brain stimulation. Trends Neurosci. 39, 782–795.
Rossi, S., Antal, A., Bestmann, S., Bikson, M., Brewer, C., Brockmöller, J., Carpenter, L.L., Cincotta, M., Chen, R., Daskalakis, J.D., 2021. Safety and recommendations for TMS use in healthy subjects and patient populations, with updates on training, ethical and regulatory issues: expert guidelines. Clin. Neurophysiol. 132, 269–306.
Rossi, S., Hallett, M., Rossini, P.M., Pascual-Leone, A., Group, S.o.T.C., 2009. Safety, ethical considerations, and application guidelines for the use of transcranial magnetic stimulation in clinical practice and research. Clin. Neurophysiol. 120, 2008–2039.
Rusu, C.V., Murakami, M., Ziemann, U., Triesch, J., 2014. A model of TMS-induced I-waves in motor cortex. Brain Stimul. 7, 401–414.
Schalk, G., 2015. A general framework for dynamic cortical function: the function-through-biased-oscillations (FBO) hypothesis. Front. Hum. Neurosci. 9, 352.
Schaworonkow, N., Nikulin, V.V., 2019. Spatial neuronal synchronization and the waveform of oscillations: implications for EEG and MEG. PLoS Comput. Biol. 15, e1007055.
Schaworonkow, N., Triesch, J., 2018. Ongoing brain rhythms shape I-wave properties in a computational model. Brain Stimul. 11, 828–838.
Schaworonkow, N., Triesch, J., Ziemann, U., Zrenner, C., 2019. EEG-triggered TMS reveals stronger brain state-dependent modulation of motor evoked potentials at weaker stimulation intensities. Brain Stimul. 12, 110–118.
Shirinpour, S., Hananeia, N., Rosado, J., Tran, H., Galanis, C., Vlachos, A., Jedlicka, P., Queisser, G., Opitz, A., 2021. Multi-scale modeling toolbox for single neuron and subcellular activity under transcranial magnetic stimulation. Brain Stimul. 14, 1470–1482.
Siebner, H.R., Funke, K., Aberra, A.S., Antal, A., Bestmann, S., Chen, R., Classen, J., Davare, M., Di Lazzaro, V., Fox, P.T., Hallett, M., Karabanov, A.N., Kesselheim, J., Beck, M.M., Koch, G., Liebetanz, D., Meunier, S., Miniussi, C., Paulus, W., Peterchev, A.V., Popa, T., Ridding, M.C., Thielscher, A., Ziemann, U., Rothwell, J.C., Ugawa, Y., 2022. Transcranial magnetic stimulation of the brain: what is stimulated? A consensus and critical position paper. Clin. Neurophysiol. 140, 59–97.
Sjöström, P.J., Turrigiano, G.G., Nelson, S.B., 2001. Rate, timing, and cooperativity jointly determine cortical synaptic plasticity. Neuron 32, 1149–1164.
Stefanou, M.-I., Desideri, D., Belardinelli, P., Zrenner, C., Ziemann, U., 2018. Phase synchronicity of μ-rhythm determines efficacy of interhemispheric communication between human motor cortices. J. Neurosci. 38, 10525–10534.
Thies, M., Zrenner, C., Ziemann, U., Bergmann, T.O., 2018. Sensorimotor mu-alpha power is positively related to corticospinal excitability. Brain Stimul. 11, 1119–1122.
Triesch, J., Zrenner, C., Ziemann, U., 2015. Modeling TMS-induced I-waves in human motor cortex. Prog. Brain Res. 222, 105–124.
van Elswijk, G., Maij, F., Schoffelen, J.-M., Overeem, S., Stegeman, D.F., Fries, P., 2010. Corticospinal beta-band synchronization entails rhythmic gain modulation. J. Neurosci. 30, 4481–4488.
Wen, H., Liu, Z., 2016. Separating fractal and oscillatory components in the power spectrum of neurophysiological signal. Brain Topogr. 29, 13–26.
Wischnewski, M., Haigh, Z.J., Shirinpour, S., Alekseichuk, I., Opitz, A., 2022. The phase of sensorimotor mu and beta oscillations has the opposite effect on corticospinal excitability. Brain Stimul. 15, 1093–1100 Basic, Translational, and Clinical Research in Neuromodulation.
Wodeyar, A., Schatza, M., Widge, A.S., Eden, U.T., Kramer, M.A., 2021. A state space modeling approach to real-time phase estimation. eLife 10, e68803.
Wolters, A., Schmidt, A., Schramm, A., Zeller, D., Naumann, M., Kunesch, E., Benecke, R., Reiners, K., Classen, J., 2005. Timing-dependent plasticity in human primary somatosensory cortex. J. Physiol. 565, 1039–1052.
Zhang, M., Frohlich, F., 2022. Cell type-specific excitability probed by optogenetic stimulation depends on the phase of the alpha oscillation. Brain Stimul. 15, 472–482.
Ziemann, U., 2020. I-waves in motor cortex revisited. Exp. Brain Res. 238, 1601.
Zrenner, B., Zrenner, C., Gordon, P.C., Belardinelli, P., McDermott, E.J., Soekadar, S.R., Fallgatter, A.J., Ziemann, U., Müller-Dahlhaus, F., 2020a. Brain oscillation-synchronized stimulation of the left dorsolateral prefrontal cortex in depression using real–time EEG-triggered TMS. Brain Stimul. 13, 197–205.
Zrenner, C., Belardinelli, P., Ermolova, M., Gordon, P.C., Stenroos, M., Zrenner, B., Ziemann, U., 2022. μ-rhythm phase from somatosensory but not motor cortex correlates with corticospinal excitability in EEG-triggered TMS. J. Neurosci. Methods 379, 109662.
Zrenner, C., Desideri, D., Belardinelli, P., Ziemann, U., 2018. Real-time EEG-defined excitability states determine efficacy of TMS-induced plasticity in human motor cortex. Brain Stimul. 11, 374–389.
Zrenner, C., Galevska, D., Nieminen, J.O., Baur, D., Stefanou, M.-I., Ziemann, U., 2020b. The shaky ground truth of real-time phase estimation. Neuroimage 214, 116761.
Zschocke, S., Hansen, H.-C., 2011. Klinische Elektroenzephalographie. Springer-Verlag.